29th Congress of the International Council of the Aeronautical Sciences
St. Petersburg, Russia; September 7-12, 2014

Numerical simulation of bird strike in aircraft leading edge structure using a new dynamic failure model

Q. Sun, Y.J. Liu, R.H, Jin
School of Aeronautics, Northwestern Polytechnical University, Xi'an 710072, China

Keywords: Bird strike; Leading edge structure; Dynamic failure model; Numerical simulations;

Abstract

Bird strike impact has become a prominent and major threat to aircraft structures, such as airplane leading edge structure. It involves the complicated progressive failure of material and structure under dynamic load with the combination effects of complex stress states, high strain rate and soft impact between bird and structure. Since the gas gun experiments of bird strikes are time consuming and costly. In consequence, it is significant to investigate the mechanism of progressive failure of structures under bird strike with the numerical simulations.

The purpose of this research paper was to perform numerical predictions of structural behavior and damage caused by bird strikes in a large airplane leading edge structure at different locations. In simulations, Smooth Particle Hydrodynamics (SPH) method was employed in bird modeling. And a novel dynamic failure model with effects of complex stress states and strain rate was implemented and appropriate contact definitions between the bird and structure were used. The results showed that the failure of leading edge structure under bird strike can be effectively simulated.

1 Introduction

Bird strike event has been one of the most dangerous risks to the safety of aircrafts. Although most bird strike event involves relatively small birds, which doesn't cause the catastrophic consequences, the possibility of severe damage generated by impacts with larger birds cannot be neglected. In order to ensure tolerance to bird strike damage, aircraft structures have to fulfill the airworthiness specifications prescribed by FAA or JAA.

Since the leading edge structure is very likely to be impacted by birds, it is very essential to research the failure mechanism of bird strikes by using numerical simulations [1-3] which could reduce, or even replace, time consuming and costly gas gun experiments on design of components of a new aircraft.

In order to deal with the numerical prediction of structural behavior and damage caused by bird strikes in an airplane leading edge structure using finite element method, interactions of several complex numerical problems including contacts [4, 5], various damage initiation and accumulation models [6-10], finite element failure and removal of failed elements, different bird modeling strategies [11-15], etc., are involved.

To simulate ductile failure of metallic leading edge structure under bird strike, the progressive dynamic failure model is involved. Johnson-Cook (J-C) model which includes constitutive relation and fracture criterion is most widely used in numerical analysis of structure under dynamic loading or impact [6, 7]. However, J-C model has some shortcomings: (1) the constitutive relation is only based on the stress-strain curve of round bar test, without considering the effects of different stress states on plasticity evolution; (2) as for the fracture criterion, only the effect of triaxiality which represents the hydrostatic stress is concerned in damage accumulation and crack initiation, ignoring the effect of Lode angle and the coupling effect of pressure and Lode angle which are reported to be the paramount factors for damage accumulation in the recent research of ductile fracture model under quasi-static

loading [8-10]. To overcome the shortcomings, a novel fracture model [9, 10] taking the effects of both stress states and strain rate on fracture under dynamic loading into consideration is applied in the present bird strike simulations.

Moreover, different bird modeling techniques have apparent effects on the results of simulations, which is essential to accurately predict the damage caused by bird strikes. There are three commonly used approaches to simulate the bird in impact: the Lagrangian approach, the Arbitrary Lagrangian Eulerian (ALE) approach [11-13] and the Smooth Particle Hydrodynamics (SPH) method. Each has different advantages over others under certain circumstances. Among them the recently developed SPH approach is gaining more and more interests in bird modeling since it could better simulate the hydrodynamic property of a bird during impact. The SPH approach is a mesh free method in which the bird is discretized by a set of discrete, mutually interacting particles. Since this approach is grid-less, it is well suited for impact problems where large distortions may occur during simulations. This method has been used to simulate the bird strike on a variety of components of aircraft structures [14, 15].

In this paper followed the SPH bird modeling approach, nonlinear bird strike simulations have been performed using explicit dynamic finite element program LS-DYNA, with the novel dynamic fracture model considering the effects of both stress states and strain rate on fracture incorporated into the user's subroutine to simulate the failure of leading edge structure due to bird strike.

2 Dynamic failure model of structures

Johnson-Cook (J-C) model which includes constitutive relation [6] and fracture criterion [7] is most widely used in numerical analysis of structure under dynamic loading or impact. The constitutive relation of J-C model reads

$$\bar{\sigma} = (A + B\bar{\varepsilon}_p^n)(1 + C\ln\dot{\bar{\varepsilon}}_p^*)(1 - T^{*m}), \quad (1)$$

where there are five material constants A, B, C, n and m. $\bar{\sigma}$ is equivalent stress, $\bar{\varepsilon}_p$ is equivalent plastic strain, the dimensionless plastic strain rate is given by $\dot{\bar{\varepsilon}}_p^* = \dot{\bar{\varepsilon}}_p / \dot{\varepsilon}_0$ where $\dot{\bar{\varepsilon}}_p$ is plastic strain rate and $\dot{\varepsilon}_0$ is the user-defined reference strain rate, the homologous temperature is defined as $T^* = (T - T_r)/(T_m - T_r)$, where T is the absolute temperature of test, and subscripts r and m indicate room and melting temperature. And the fracture criterion of J-C model is written as

$$\varepsilon_f = [D_1 + D_2 \exp(\frac{D_3\sigma_m}{\bar{\sigma}})](1 + D_4 \ln\dot{\bar{\varepsilon}}_p^*)(1 + D_5 T^*), \quad (2)$$

where D_1, D_2, D_3, D_4, and D_5 are material constants. $\sigma_m = -p = (\sigma_1 + \sigma_2 + \sigma_3)/3$ is mean stress or hydrostatic stress where p is hydrostatic pressure. The dimensionless mean stress is also commonly used in literature and is defined as the triaxiality, $\eta = \sigma_m / \bar{\sigma}$.

However, J-C model ignores the effect of Lode angle and the coupling effect of pressure and Lode angle on the plastic evolution and damage initiation which are reported to be the paramount factors in the recent research of ductile fracture model under quasi-static loading.

In the present paper, a novel fracture model taking the effects of both stress states and strain rate on fracture under dynamic loading into consideration is applied in bird strike simulations. The details of the fracture model including constitutive evolution and fracture criteria are in the references [9, 10].

2.1 Constitutive evolution

Without considering the temperature effect, the constitutive relation is formerly regarded as the function of equivalent stress with respect to plastic strain $\bar{\varepsilon}_p$, plastic strain rate $\dot{\bar{\varepsilon}}_p^*$. However, recent research revealed that the stress-strain relation is also changed with different stress states, i.e., the change of triaxiality η (or pressure) and Lode angle θ_L. As a result, the constitutive relation should be written as

$$\bar{\sigma} = g(\bar{\varepsilon}_p, \dot{\bar{\varepsilon}}_p, \eta, \bar{\theta}), \quad (3)$$

where $\bar{\theta}$ is Lode angle parameter and defined as

$$\bar{\theta} = -\frac{6\theta_L}{\pi}. \quad (4)$$

The parameter $\bar{\theta}$ ranges from -1 to 1 in which the typical values, $\bar{\theta} = -1$, $\bar{\theta} = 0$ and $\bar{\theta} = 1$,

represent generalized compression, shearing and tension, respectively. As $\bar{\theta}$ is the normalized Lode angle, the parameter $\bar{\theta}$ will be also called the Lode angle hereinafter.

Our former research has revealed that triaxiality has significant effect on initial yield stress while Lode angle is important in subsequent yield condition [10]. The expression for the constitutive relation reads

$$\sigma_{yld} = \sigma_{y0} \cdot [1 + k(\eta - \frac{1}{3})], \quad (5)$$

$$H_r = H(\bar{\varepsilon}_p) \cdot [1 + w(1 - |\bar{\theta}|)], \quad (6)$$

where

$$H(\bar{\varepsilon}_p) = \frac{d\sigma(\bar{\varepsilon}_p)}{d\bar{\varepsilon}_p}. \quad (7)$$

In the above relation, the modified initial yield stress σ_{yld} and tangent slope H_r are based on the original initial yield stress σ_{y0} and tangent slope H which can be obtained from the result of smooth round tensile bar test. For the convenience of numerical simulations, $\sigma(\bar{\varepsilon}_p)$ is fitted with a power law function from the true stress-strain curve of smooth round tensile bar test up to the necking point and extrapolated beyond necking. We assume that the strain hardening obeys the following three parameter rule,

$$\sigma(\bar{\varepsilon}_p) = \sigma_{y0} + K\bar{\varepsilon}_p^n, \quad (8)$$

where σ_{y0}, K, n are material constants. Considering the strain rate effect and combining Eqs. (5) – (7), the novel constitutive relation has the form,

$$\sigma_{yd} = \sigma_y(1 + C\ln\dot{\bar{\varepsilon}}_p^*), \quad (9)$$

where

$$\sigma_y = \sigma_{y0}[1 + k(\eta - \frac{1}{3})] + K[1 + w(1 - |\bar{\theta}|)]\bar{\varepsilon}_p^n. \quad (10)$$

In Eq. (9), C is the strain rate sensitivity constant. This novel constitutive relation extends the J-C model by involving the influence of different stress states on plasticity evolution.

2.2 Fracture criteria

Pressure (or triaxiality) and Lode angle have proven to be important in ductile fracture under complex stress states and quasi-static loading condition. As for dynamic loading, the effect of strain rate should be considered into fracture criteria. The general form can be written as

$$\varepsilon_f = f(\eta, \bar{\theta}, \dot{\bar{\varepsilon}}_p). \quad (11)$$

Based on our recently proposed quasi-static fracture criterion [9] and by considering the effect of strain rate, the present dynamic fracture criterion is,

$$\varepsilon_{fd} = \varepsilon_f \cdot \mu_d, \quad (12)$$

where μ_d is term of strain rate

$$\mu_d = (1 + D\ln\dot{\bar{\varepsilon}}_p^*), \quad (13)$$

D is the strain rate sensitivity constant and ε_f is the quasi-static fracture envelope,

$$\begin{cases} \varepsilon_f = \varepsilon_{f0} \cdot \mu_1(p, \bar{\theta}) \cdot \mu_2(\bar{\theta}, p) \\ \mu_1(p, \bar{\theta}) = (1 + \dfrac{p}{p_{lim} - p})^{a(\bar{\theta})} \\ a(\bar{\theta}) = (a_0 - b_0) \cdot \bar{\theta}^2 + b_0 \\ \mu_2(\bar{\theta}, p) = \gamma + (1 - \gamma)|\bar{\theta}|^{c(p)} \\ c(p) = -\dfrac{1}{2}\tanh[c_0 \cdot (p - p_0)] + \dfrac{1}{2} \end{cases}. \quad (14)$$

The details of the fracture model for quasi-static loading are in the reference [10].

2.3 Damage accumulation

Based on the damage mechanics, the damage of ductile material can be characterized as the relative loss of its plasticity. And the accumulation of damage is associated with its current stress state. The most widely used damage accumulation method is linear accumulation method which reads

$$D(\varepsilon_p) = \int_0^{\varepsilon_p} \frac{1}{\varepsilon_{fd}} d\varepsilon_p, \quad (15)$$

where D is the value of damage at current plastic strain ε_p, ε_{fd} is the fracture plastic strain at current stress state. When $\varepsilon_p = \varepsilon_c$, i.e. $D=1$, the material fails and ε_c is the final fracture plastic strain.

3 Numerical Modeling

In this section, the discretization of the leading edge structure and the bird is introduced. The contact and connection conditions between the different components of the structure are properly set in simulations.

3.1 FE model of Leading edge structure

The leading edge structure mainly contains: outer skin, inner skin, front wall, leading edge ribs (49 pieces) and front spar. The skins and interior structure are showed in Fig. 1. The whole leading edge structure is made of AL7075.

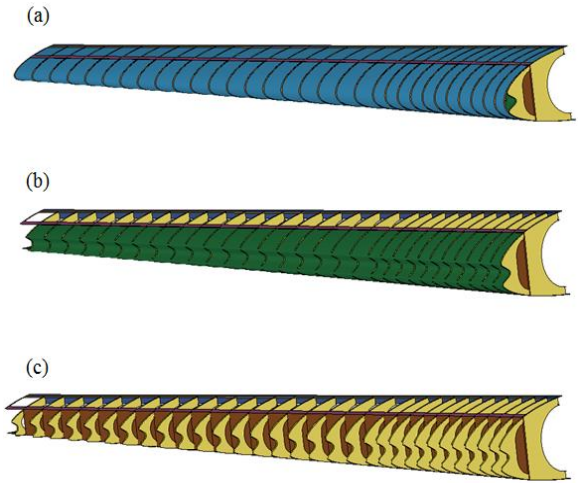

Fig.1. Leading edge structure (a) outer skin (b) inner skin and (c) interior structure.

Due to the geometric property, shell elements with different thicknesses are used in building the various parts of the FE model of leading edge structure. In order to accurately capture the local failure during the impact, the element size is properly chosen through sensitivity analysis of mesh size, which will be illustrated in section 4. The details of discretization of skins and interior structure are showed in Fig. 2.

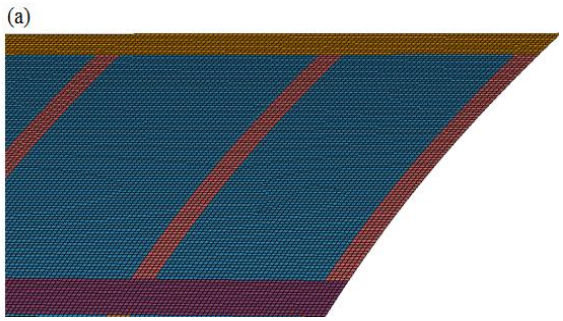

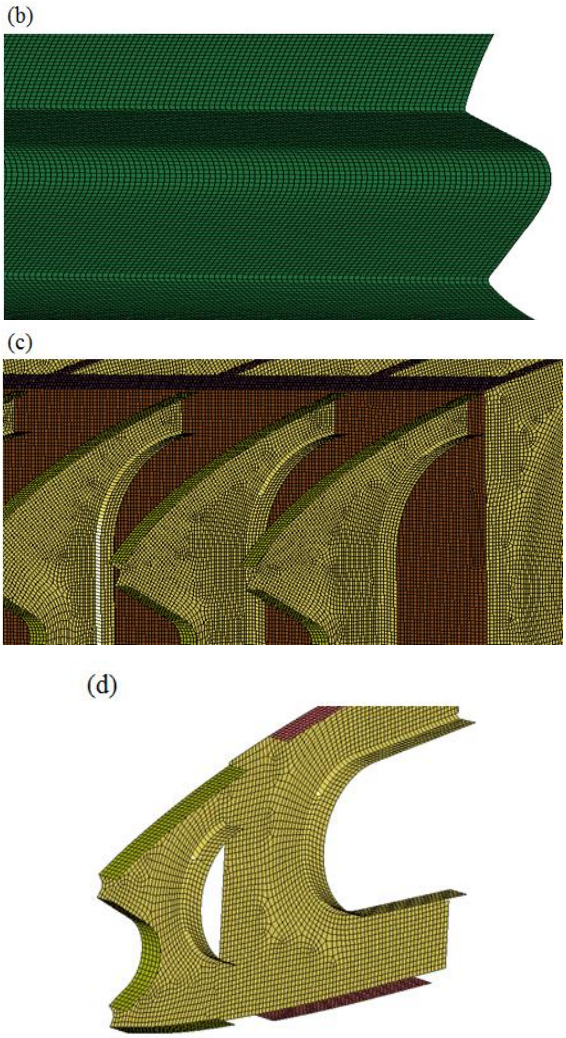

Fig.2. Detailed meshes of components of leading edge structure (a) outer skin, (b) inner skin, (c) interior structure and (d) rib.

In order to lead a relatively conservative numerical result, strict boundary constraints with the three translational degrees of freedom fixed at the top and bottom flanges of front spar are adopted, which is illustrated in Fig. 3(a). Moreover, different parts of the structure are assembled together by proper connection techniques which can be seen in Fig. 3(b). The parts of interior structure are connected by sharing the same nodes. However, the rivet connections between skins and interior structure are modeled through nodal split with tie break failure criterion in LS-DYNA which has

$$\left(\frac{|f_n|}{NFLF}\right)^{NEN}+\left(\frac{|f_s|}{SFLF}\right)^{MES}\geq 1, \qquad (16)$$

where *NFLF* denotes the tension strength, *SFLF* denotes the shear strength, the NEN and MEN

are parameters which are usually selected as 2, f_n and f_s are represented as the tension and shear between the two connected nodes respectively. Other non-rivet connected nodes between skins and interior structure employs specific surface to surface contact condition. And the contact between bird and structure is well set.

In simulation of structural failure due to strike, the material constants of AL7075 in novel dynamic failure model is listed in Tables 1 and 2.

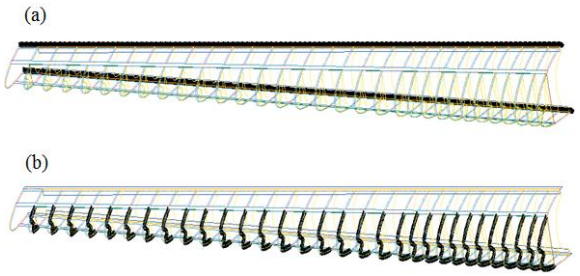

Fig.3. Boundary conditions of leading edge structure (a) fixed conditions at the top and bottom flanges (b) connection conditions between skins and interior structure.

Table 1. Al 7075 material constants in the constitutive relation of the novel model

Yield stress and strain hardening					Strain rate hardening	
σ_{y0} (MPa)	K (MPa)	n	k	w	$\dot{\varepsilon}_0$ (s^{-1})	C
420	326	0.23	-0.30	-0.20	10^{-4}	0

Table 2. Al 7075 material constants in the fracture criterion of the novel model

	μ_1			μ_2			μ_d	
ε_{f0}	$p_{\lim}$ (MPa)	a_0	b_0	γ	c_0	p_0	$\dot{\varepsilon}_0$ (s^{-1})	D
0.78	1200	5.95	1.52	0.20	0	0	10^{-4}	-0.0085

3.2 Bird modeling

In the present paper, the smooth particle hydrodynamics (SPH) method [14, 15] is adopted to model the bird. In the SPH method, the equations of motion are constructed with the Lagrangian formulation. However, instead of a grid, kernel functions (radius basis functions, i.e., RBFs) are used to calculate the field variables at each particle. The kernel function is active only over a given volume around each node. Each node has a given mass and constitutes an element in the sense that the state variables are evaluated at its location. The method is said to be mesh free because there is no predefined grid restraining which nodes can interact together.

In bird modeling with SPH technique, The SPH bird model is assumed to simulate the uniform material behavior instead of the heterogeneous nature of a bird.

A hydrodynamic model with failure strain criterion is adopted to represent the behavior of the bird. The material constants of elastoplastic constitutive relation of the bird are listed in the Table 3. When the failure strain is reached, the SPH particle is deleted in analysis. And the Equation of State (EOS) used for the bird is the polynomial relation between density and hydrostatic stress,

$$P = C_0 + C_1\mu + C_2\mu^2 + C_3\mu^3 + (C_4 + C_5\mu + C_6\mu^2)E \quad , \tag{17}$$

where P is the pressure, μ is the ratio of the current density to the reference density, E denotes the internal energy, and C_i are the material constants which are selected as C_1=2250MPa and C_0= C_2=…= C_6= 0 in this research.

In simulations, the geometry of the bird is a cylindrical body of 2:1 in length: diameter ratio with spherical end caps (Fig. 4). And its mass is adopted as 3.6 kg. The size of the SPH particles

is carefully adopted in analysis. In order to determine the proper SPH particle size in bird strike simulation of the leading edge structure, sensitivity analysis of SPH particle size is performed, which will be demonstrated in section 4.

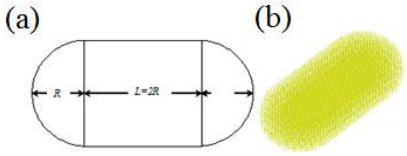

Fig. 4. Geometry (a) and the SPH model (b) of a bird

Table 3. Material constants of bird.

Elasitic modulus (GPa)	Possion's ratio	Density ($kg.m^{-3}$)	Yield stress (MPa)	Tangent modulus (MPa)	Failure strain	Hardening coefficient
10.0	0.3	950	1.0	5.0	1.25	1

4 Effects of element discretization

In order to evaluate the effect of element size on the results of impact FE analyses, calibrations of discretization size of structure (shell element) and SPH particle have been performed.

4.1 Discretization of SPH particle

In calibration, the SPH bird impacts on the target plate are performed. The size of target plate is $600mm \times 600mm \times 2mm$ which is meshed in shell elements with discrete size $6mm$. Different impact velocities of bird and discretization of SPH particle are selected. The mass of bird is $3.6kg$, and the initial velocities, i.e. $80m/s$, $125m/s$ and $170m/s$, and three cases of discrete size (Fig. 5), i.e. $0.1957cm^3$ (case 1, 9908 particles), $0.0521cm^3$ (case 2, 37217 particles) and $0.02377cm^3$ (case 3, 81573 particles), are adopted.

Numerical results of maximum contact force for different cases are listed in Table 4. The differences of numerical results due to the different particle size at each impact velocity are less than 1%. The relative difference of maximum contact force for the three velocities between cases 2 and 3 is 0.85%, 0.85% and 0.74%, respectively. Considering the numerical efficiency, the particle size in the case 2, i.e. $0.0521cm^3$, is adopted in the following simulations.

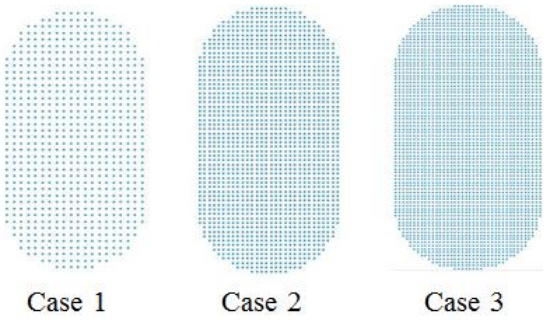

Fig. 5. Different discrete sizes of SPH particles

Table 4. Maximum impact force for the different discretization of SPH bird at different velocities.

	Case 1 (10^6 N)	Case 2 (10^6 N)	Case 3 (10^6 N)
80 m/s	0.125111	0.123943	0.1250042
125 m/s	0.2150643	0.2175301	0.2157073
170 m/s	0.3283318	0.3447723	0.3473512

4.2 Discretization of shell element

Furthermore, in order to verify the different mesh size of shell element of structure on the numerical results, discrete sizes with $3mm$, $6mm$, $8mm$, $10mm$ and $15mm$ of pate are selected. In impact simulations, the mass of bird is still $3.6kg$ with a velocity of $170m/s$ and the discretization size of SPH particle in bird modeling is selected as the $0.0521cm^3$ (case 2). The numerical results of deformation and failure are shown in Fig. 6.

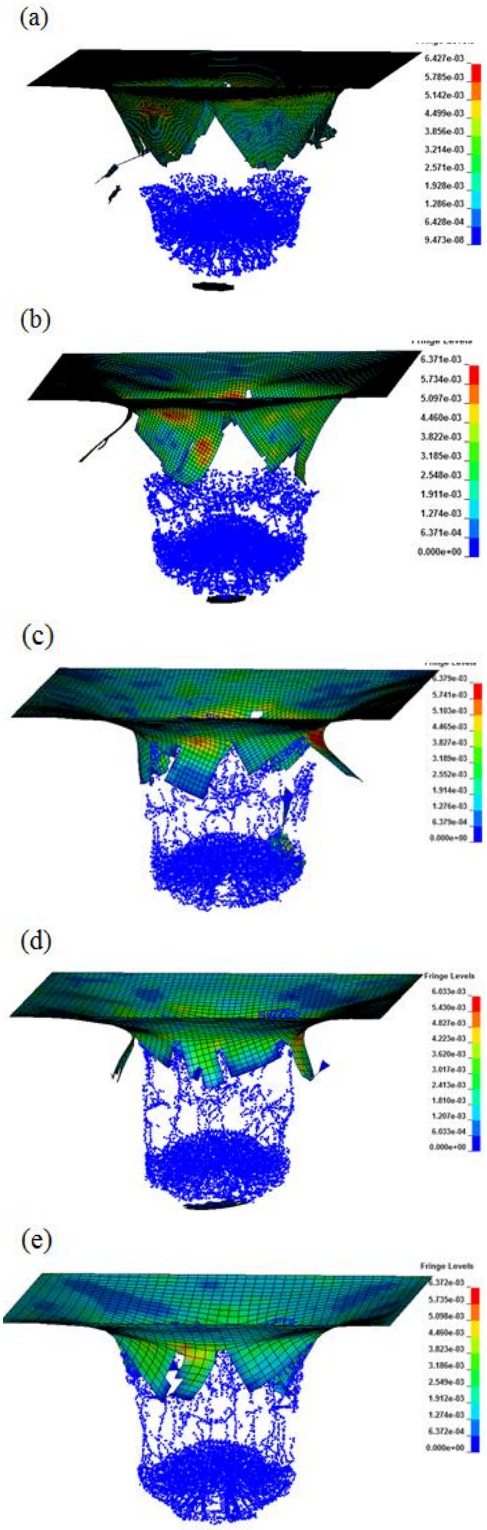

Fig. 6. Different discrete mesh sizes of shell elements: (a) 3*mm*, (b) 6*mm*, (c) 8*mm*, (d) 10*mm* and (e) 15*mm*.

During the impact, the maximum ratio of hourglass energy to the internal energy for the different meshes as well as the corresponding time is listed in Table 5.

Table 5. The ratio of hourglass energy to the internal energy and computational time for the different mesh sizes.

Mesh size (*mm*)	Hourglass energy/internal energy (%)	Computational time (*min*)
15	6.2	2
10	4.4	4
8	3.6	5
6	2.8	7
3	1.3	29

Generally, the numerical results using reduced integrated elements can be accepted if the ratio of hourglass energy to the internal energy is controlled below 10%, and it would has relatively high accuracy if this ratio is below 5%. Moreover, since the stable increment is associated with the mesh size, it would be consuming as the mesh size is decreasing in explicit analysis.

By considering both the computational time and the accuracy, it can be seen from Table 5 that the mesh size below 6*mm* can be adopted in the bird strike simulation of aircraft leading edge.

5 Simulations of bird strikes

In this section, numerical simulations of bird strikes on the leading edge structure have been performed using explicit dynamic finite element program LS-DYNA. In simulations, three striking locations are selected along the span wise of the leading edge.

The location 1 is on the rib (25#) located near the root of the wing, the location 2 is on the rib (34#) located near the middle of the wing and the location 3 is on the rib (48#) located at the tip of the wing, which are shown in Fig. 7.

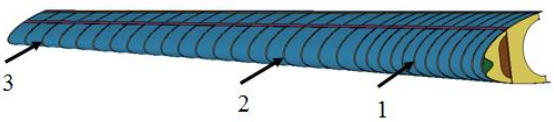

Fig. 7. Impact locations on the leading edge structure

The weight of bird is also set to be 3.6*kg*, the initial speed is 125*m/s* and the initial kinetic energy is 28155.5*J*. The angle between the speed and the cord line is 85°.

Fig. 8 shows the history of kinetic energy during the bird strike and Fig. 9 shows the corresponding evolution of contact force between bird and structure. Numerical results show that the residual kinetic energy for the three locations at 5*ms* is below 1% of the initial energy 28155.5*J*, which indicates that the striking process is completed at 5*ms* for all of the three locations. The kinetic energy at 5*ms* is listed in the Table 6.

Table 6. The residual kinetic energy at 5*ms*

Location 1	Location 2	Location 3
133.8*J* (0.48%)	211.8*J* (0.75%)	126.8*J* (0.45%)

The kinetic energy for all of the three cases decreases at almost the same rate at the beginning (before 2*ms* in Fig. 8), but have apparent differences after 2*ms*. It can be seen that the energy decreasing rate slows down as the striking position moving near the tip of the leading edge structure. And from the contact force history (Fig. 9) we can see that significant difference of contact force has also appeared after 2*ms*. As the striking position moving toward the tip, the contact force is decreasing, which reveals the absorption property of kinetic energy deteriorates if bird impact occurs at the tip. Such conclusion can also be verified by the deformation of leading edge structure after strike at the three positions (Fig. 10).

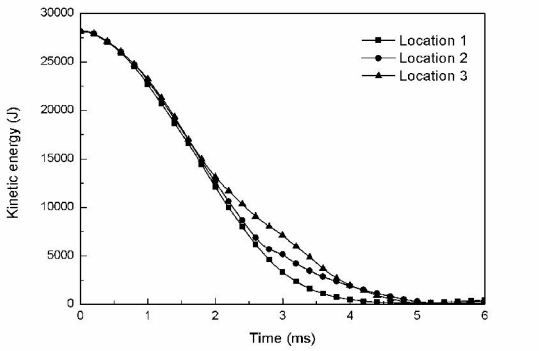

Fig. 8. The history of kinetic energy during striking at the three locations

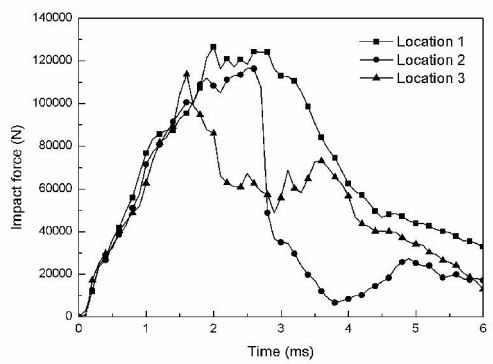

Fig. 9. The history of impact force during striking at the three locations

Numerical results of deformations show that the impact influenced region is confined within the region of 4 ribs from the strike point, i.e. totally 9 ribs, are in plasticity due to strike at the location 1. While the impact influenced region is confined within the 2 ribs from the strike point, i.e. totally 5 ribs, are in plasticity due to strike at the location 2. And there are 4 ribs are in plasticity at location 3. In consequence, the size of plastic deformation region at location 1 is larger than that at locations 2 and 3. The different size of plastic deformation region also verifies that the kinetic energy absorption near the root of the present leading edge structure is higher than those away from the root.

Moreover, splitting and tearing of outer skin from the rib at the impact position can be observed for bird strikes at locations 2 and 3. And the numerical results also show that sever plastic deformation is occurred in leading edge ribs and skins, but there is no plastic deformation in front wall, which shows that it is hard for bird to penetrate the front wall. This result also reveals that the impact energy is almost absorbed by the large-scale plastic deformation of outer skins (including some parts of leading edge ribs).

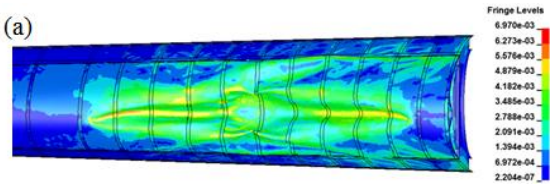

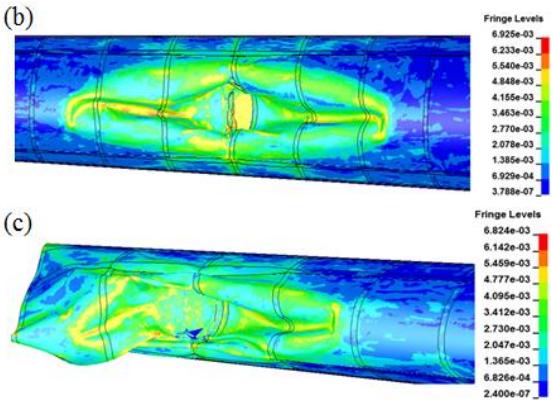

Fig. 10. The deformation of leading edge structure after strike at: (a) location 1, (b) location 2 and (c) location 3.

6 Conclusions

In the present paper, numerical failure prediction of bird strike on an aircraft leading edge structure was simulated in LS-DYNA. In strikes, a novel dynamic ductile fracture model was involved and implemented to simulate failure of structure. This fracture model combines the effects of strain rate and stress states including pressure and Lode angle on the damage evolution. The SPH technique was used in modeling hydrodynamic property of bird.

Furthermore, in order to obtain reliable numerical results, the sensitivity analyses of the discrete sizes including the size of shell element in structure and the size of SPH particle in bird were conducted to calibrate the size of discretization.

With the calibrated discretization, simulations of bird strike on an aircraft leading edge structure at three different locations along with the span of wing were performed. Numerical results showed that the impact damage is dependent on the impact location. It can be concluded that the capacity of kinetic energy absorption near the root of the present leading edge structure is higher than those away from the root, since the plastic deformation involved regions decrease from wing root to tip for the present leading edge structure.

Acknowledgements

This research was supported by the Doctorate Foundation of Northwestern Polytechnical University (CX201301).

References

[1] Guida M, Marulo F, Meo M, et al. Analysis of bird impact on a composite tailplane leading edge. Applied Composite Materials, Vol. 15, No. 4-6, pp 241-257, 2008.

[2] Smojver I, Ivančević D. Numerical simulation of bird strike damage prediction in airplane flap structure. Composite structures, Vol. 92, No. 9, pp 2016-2026, 2010.

[3] Wang F S, Yue Z F. Numerical simulation of damage and failure in aircraft windshield structure against bird strike. Materials & Design, Vol. 31, No. 2 pp 687-695, 2010.

[4] Hanssen A G, Girard Y, Olovsson L, et al. A numerical model for bird strike of aluminium foam-based sandwich panels. International Journal of Impact Engineering, Vol. 32, No. 7, pp 1127-1144, 2006.

[5] Airoldi A, Cacchione B. Modelling of impact forces and pressures in Lagrangian bird strike analyses. International Journal of Impact Engineering, 2006, Vol. 32, No. 10, pp 1651-1677, 2006.

[6] Johnson G R, Cook W H. A constitutive model and data for metals subjected to large strains, high strain rates and high temperatures. Proceedings of the 7th International Symposium on Ballistics, Vol. 21, pp 541-547, 1983.

[7] Johnson G R, Cook W H. Fracture characteristics of three metals subjected to various strains, strain rates, temperatures and pressures. Engineering fracture mechanics, Vol. 21, No. 1, pp 31-48, 1985.

[8] Xue L, Wierzbicki T. Numerical simulation of fracture mode transition in ductile plates. International Journal of Solids and Structures, Vol. 46, No. 6, pp 1423-1435, 2009.

[9] Liu Y J, Sun Q, Fan X L, et al. A stress-invariant based multi-parameters ductile progressive fracture model. Materials Science and Engineering: A, Vol. 576, pp 337-345, 2013.

[10] Liu Y J, Sun Q. A dynamic ductile fracture model on the effects of pressure, Lode angle and strain rate. Materials Science and Engineering: A, Vol. 589, pp 262-270, 2014.

[11] Lavoie M A, Gakwaya A, Ensan M N, et al. Review of existing numerical methods and validation procedure available for bird strike modeling. International conference on computational & experimental engineering and sciences, Vol. 2, pp 111-118, 2007.

[12] Liu Y, Li Z, Sun Q, et al. Separation dynamics of large-scale fairing section: a fluid–structure interaction study. Proceedings of the Institution of

Mechanical Engineers, Part G: Journal of Aerospace Engineering, Vol. 227, No. 11, pp 1767-1779, 2013.
[13] Jain R, Ramachandra K. Bird impact analysis of pre-stressed fan blades using explicit finite element code. Proceedings of the International Gas Turbine Congress Tokyo. 2003.
[14] Guida M, Marulo F, Meo M, et al. SPH–Lagrangian study of bird impact on leading edge wing. Composite Structures, Vol. 93, No. 3, pp 1060-1071, 2011.
[15] Liu J, Li Y L, Xu F. The numerical simulation of a bird-impact on an aircraft windshield by using the SPH method. Advanced Materials Research, Vol. 33, pp 851-856, 2008.

Contact Author Email Address

lyanjie@mail.nwpu.edu.cn (Y.J. Liu)

Copyright Statement